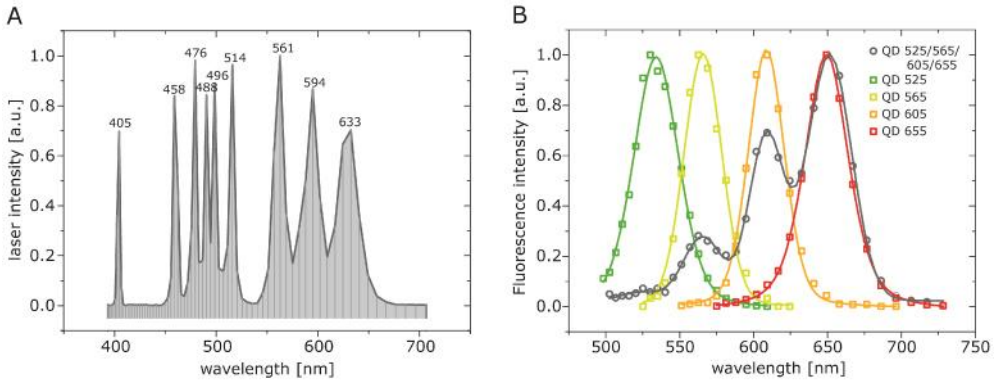


Fig. 2. Spectral calibration. (A) Laser lines reflected at a coverglass in front of the objective lens. The nonlinear dispersion of the prism results in a distribution of data points that is not linear with the wavelength. (B) Measured time integrated intensity spectra of the mixed and separate QD solutions (open symbols) and fits of Gaussian curves (solid lines).

increasing QD crystal size [29] resulting in the different peak heights of the emission maxima in the mixture. We could fit a sum of 4 Gaussian curves to the intensity spectrum, which corresponded in width and position to the fits of single Gaussian curves to the spectra of the separate solutions.

*4.3 Comparison of FCS measurements acquired with the EMCCD and with APDs*

We used a 20 nM solution of Alexa 488 and a 25 nM solution of QD 655 in order to compare FCS measurements taken with the EMCCD-based spectrometer and with the APD-based filter setup. For Alexa 488 we chose a spectral range of 500-551 nm whereas for QD 655 we chose 608-682 nm in order to match the properties of the filters used. Figure 3A and B show that the ACFs are very similar for the two setups with the major difference that the time resolution of the EMCCD is limited to 12 µs. From a single component free diffusion fit (i.e. $\alpha = 1$ and $f_1 = 1$) of Eq. (2) to the data very similar diffusion correlation times could be obtained, showing that we get substantially the same results with both setups.

In order to assess the concentration range accessible with the setup we acquired FCS data from a concentration series of QD 655 covering 1-50 nM with constant laser intensity. The number of molecules in the focal volume $N$ resulting from the fits of Eq. (2) to the data showed an almost linear dependence on the concentration, see Fig. 3C, supported by a fit of a power law to a double-logarithmic representation of the data that yielded a slope of 1.06±0.04. Only for relatively small concentrations below 2 nM we observed a deviation from linearity due to an increasing influence of the background signal.

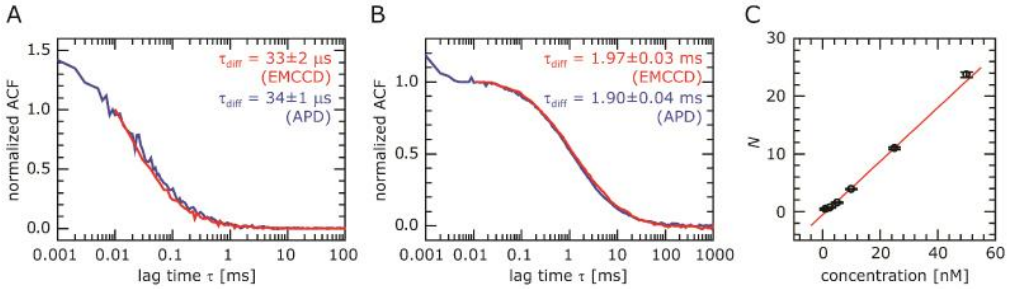


Fig. 3. Comparison with APD measurements. ACFs of Alexa 488 (A) and of QD 655 (B) in solution measured with the APD-based (blue) and with the EMCCD-based setup (red) normalized to the values at 12 µs lag time. The initial decrease at lag times <10 µs of the APD-based ACF of QD 655 was probably due to additional triplet state occupation and excluded for the fit. The diffusion correlation times from the fits are in good agreement. (C) Number of molecules in the focus as obtained from the fit of FCS data of QD 655 plotted against the concentration of the solution (black circles) and linear fit (red line).

## 5. Spectrally resolved FCS measurements

### *5.1 FCS of a mixture of QDs*

From full spectral intensity time traces acquired in the equimolar mixture solution, see Fig. 2B, channel intensity time traces were extracted by binning over the wavelength windows 507-540 nm, 546-582 nm, 588-625 nm, and 633-696 nm corresponding to the FWHM of the emission profiles of the single QD species. The channel intensity time traces were then subject to an autocorrelation analysis, see Fig. 4A. From an integration of the emission spectra of the single QD species over the channel windows weighted with the peak intensities in the mixture (Fig. 2B), the cross-talk of the different species into channels assigned to the other species could be determined: the signal in the first window was composed to 85% of QD 525 emission and to 15% of QD 565 emission; in the second channel, the contributions were 9% QD 525, 83% QD 565, 8% QD 605; in the third channel, 4% QD 565, 79% QD 605, 17% QD 655; and in the fourth channel, 6% QD 605; 94% QD 655. Since in an ACF, different species are weighted with the square of the brightness per particle, the cross-talk-induced contributions to the ACFs amounted to not more than $(0.17/0.79)^2 \approx 5\%$. Therefore, fits with a single freely diffusive component and an exponential blinking contribution, i.e. $\alpha = 1$ and $f_1 = 1$ in Eq. (2), were justified and resulted in diffusion correlation times that increased with increasing maximum emission wavelength, see Fig. 4B. For an estimation of the expected spectral dependence of the diffusion correlation times we used the radii of gyration of 6, 7, 8 and 9 nm (values provided by the manufacturer) for QD 525, 565, 605 and 655, respectively, including core, shell and polymer coating of the QDs. We estimated the additional chromatic contribution based on the fact that a constant pinhole size was used for the complete spectrum and on the assumption that the focal radius $w_0$ depends on the illumination and the detection wavelengths $\lambda_{ill/det}$ according to

$$w_0^2 \propto \lambda_{ill}^2 + \lambda_{det}^2 \quad \text{so that} \quad \tau_{diff} \propto \left(1 + \frac{\lambda_{det}^2}{\lambda_{ill}^2}\right) R_i, \quad N \propto \left(1 + \frac{\lambda_{det}^2}{\lambda_{ill}^2}\right)^{3/2} \tag{5}$$

[25] and using the value of QD 525 as reference. Measured and theoretically expected diffusion correlation times agreed well with the exception of QD 655. The spectral dependence cannot be explained with either the chromatic or the size dependence alone so that we are indeed able to distinguish the 4 species present in the same solution. Different properties of photophysical effects such as blinking may have affected the apparent diffusion correlation times because it can be difficult to distinguish diffusional and photophysical contributions to the fluctuations when they occur on similar time scales [30], thus leading to the observed deviation of theory and experiment especially for QD 655. This may result from underestimating the contribution of blinking, thus yielding an underestimation of the diffusion correlation time. Therefore, QD 655 was studied in more detail.

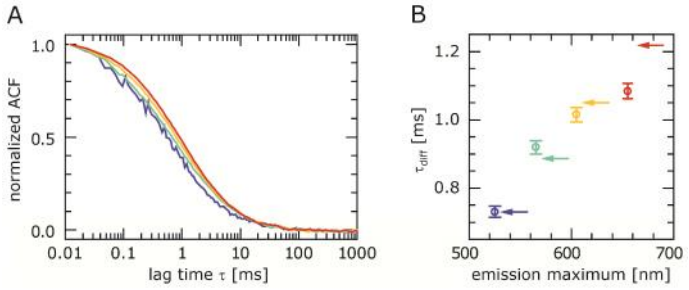


Fig. 4. FCS of a mixture of QDs. (A) ACFs of QD 525 (blue), 565 (green), 605 (yellow), and 655 (red) based on time trace extracted from a full spectral intensity recording by binning over appropriate detection windows. (B) The resulting diffusion correlation times for the respective QDs as a function of the maximum emission wavelength (circles) and the spectral dependence as theoretically expected from size and chromatic effects (arrows).

#131620 - $15.00 USD Received 13 Jul 2010; revised 29 Sep 2010; accepted 1 Oct 2010; published 27 Oct 2010

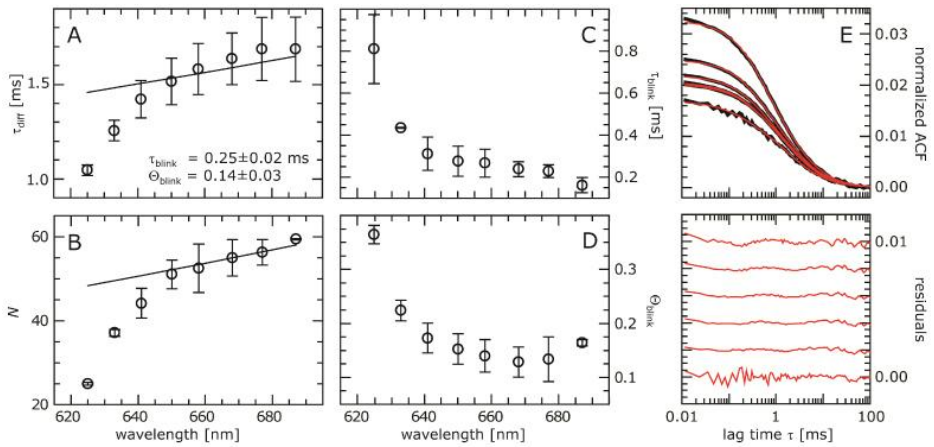


Fig. 5. Spectrally resolved diffusion and fluorescence intermittence of QD 655. Spectral dependence of (A) the diffusion correlation time and (B) the number of molecules in the focal volume (circles) from fits with globally linked blinking parameters. The estimated chromatic dependence (solid lines) is based on the interpolated values at 655 nm. Spectral dependence of (C) the blinking correlation time and (D) the fraction in a non-fluorescent state from fits applying the estimated chromatic dependence from (A) and (B). Error bars are obtained from averaging over 4 experiments. (E) The measured ACFs (black) and the fits (red) resulting in (C) and (D) and the corresponding residuals for the data points 625, 633, 641, 649, 667 and 686 nm (top to bottom). The residuals were shifted by 0.002 each for better legibility. The qualitiy of the fits was similar for both approaches.

### *5.2 Spectrally resolved fluorescence intermittence of QD 655*

In a next step, we restricted the FCS analysis to spectral intensity recordings of QD 655 in solution for a better assessment of the different contributions to the spectral dependence of the ACFs. We extracted time traces binned over ~17 nm windows centered at 625, 633, 641, 650, 658, 668, 677, and 686 nm and fitted the ACFs computed therefrom globally with linked blinking parameters and individual amplitudes and diffusion parameters using the same model as before in order to account for the expected chromatic size dependence of the focal volume, see Fig. 5A and B. In order to compare the outcome with the expected chromatic dependence, we extrapolated the diffusion correlation time and the number of molecules as described in the previous section and based on the values for 655 nm, i.e. the emission maximum. Whereas above 655 nm, the values followed the estimated behaviour, both the diffusion correlation time and the number of molecules were significantly smaller than the prediction for shorter wavelengths. This is indicative for higher populated and longer-lived non-fluorescent states because it can be difficult to distinguish diffusional from photophysical contributions when they occur on similar time scales when fitting correlation functions. Underestimating the fraction of molecules in a dark state can result in an artificial underestimation of the total number of molecules, and underestimating the lifetime of the dark states can result in an artificial underestimation of the diffusion correlation time. When fitting with all parameters kept independent, we obtained an intermediate result where $\tau_{diff}$ and $N$ showed a spectral dependence stronger than the prediction and also $\tau_{blink}$ and $\theta_{blink}$ varied with the wavelength. Therefore, we repeated the fitting with the number of molecules and diffusion correlation times following the estimated spectral dependence (solid lines in Fig. 5A and B) whereas the blinking correlation time and the fraction of non-fluorescent particles were free parameters, see Fig. 5C, D and E. Both parameters decreased with increasing wavelength and approached a plateau above 655 nm. That way we made use of the spectral resolution to obtain information that is not accessible with a conventional FCS setup.

This observation is in agreement with previous studies stating that fluorescence intermittence of QDs cannot be described sufficiently with single characteristic transition rates to and exponential ACFs of the occupation of non-fluorescent trap states [30–33]. Our observations suggest that excitation into electronic levels farther above the energy gap of the

#131620 - $15.00 USD Received 13 Jul 2010; revised 29 Sep 2010; accepted 1 Oct 2010; published 27 Oct 2010

semiconductor crystal (as indicated by the shorter emission wavelength) result not only in a higher energy of the photons created upon electron-hole recombination but also in a higher probability to occupy trap states that have in addition longer lifetimes. This will be subject of a more detailed study.

*5.3 Spectrally resolved FCCS in living cells*

To assess the usability of our setup for live cell FCS and FCCS experiments, we used MCF7 cells either expressing a fusion protein containing EGFP and two mRFP copies [26] or co-expressing EGFP and mRFP as positive and negative control, respectively, for FCCS, see Fig. 6A. Using the conventional APD-based filter setup we could confirm a pronounced cross-correlation for the positive control with ratioG = 0.44±0.04 and the substantial absence of cross-correlation for the negative control with ratioG = 0.04±0.03, see Fig. 6B. In general, ratioG is obtained from fits of the ACFs and the CCF and Eq. (3).

After replacing the APD-based setup by the EMCCD-based spectrometer we repeated the experiments by reading complete spectral intensity traces. The data were binned either into two discrete channels at 504-540 nm (assigned to EGFP) and 617-696 nm (mRFP) or binned over ~16 nm into 6 spectral channels, three of which were assigned to EGFP and centered at 512, 521 and 530 nm, whereas the other three were assigned to mRFP and centered at 603, 618 and 633 nm. The cross-correlations obtained with the discrete channels that were similar to the properties of the filters used before were in good agreement with the APD-based measurements with ratioG = 0.39±0.03 and 0.07±0.02 for the positive and the negative control, respectively, see Fig. 6C.

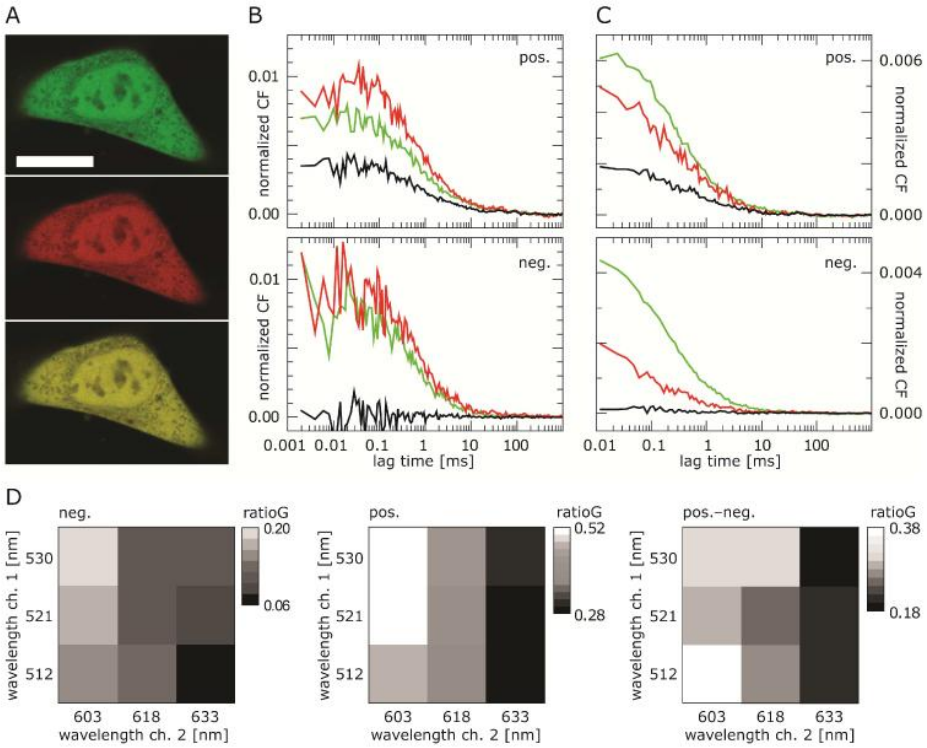


Fig. 6. Spectrally resolved FCCS in living cells. (A) Confocal images of a positive control MCF7 cell showing the EGFP (green) and the mRFP (red) fluorescence and an overlay image (yellow), scale bar 20µm. (B) ACFs of the EGFP (green) and the mRFP fluorescence signal (red) as well as their CCF acquired in positive (pos.) and negative control (neg.) MCF7 cells with the APD-based filter setup. (C) The same as in (B), but acquired with the EMCCD-based spectrometer setup. (D) ratioG values determined for 3×3 spectral windows from data acquired in positive (pos.) and negative (neg.) control cells and their difference (pos.-neg.).

#131620 - $15.00 USD Received 13 Jul 2010; revised 29 Sep 2010; accepted 1 Oct 2010; published 27 Oct 2010

Then we determined the auto- and cross-correlations and the corresponding ratioG values for all 9 combinations of the narrow band channels, see Fig. 6D. As expected, the closer the detection windows were, the higher was the cross-talk-induced cross-correlation in the negative control and the higher was also the overall cross-correlation in the positive control, and vice versa. The difference of the ratioG values therefore defines the useful accessible dynamic range for measuring interactions which was maximal for the shortest wavelength windows for both fluorophores. Thus, for EGFP/mRFP-based FCCS experiments it is more important to match the emission maximum with the detection window than to reduce cross-talk but risk to lose signal at the same time.

## 6. Conclusion

Fluorescence correlation spectroscopy is a powerful tool now widely employed in biochemistry and cell biology to measure diffusion and interaction properties of biomolecules. We present here the successful implementation of an EMCCD- and prism-based spectrometer for spectrally resolved FCS that combines the advantages of a prism, i.e. high transmission and robust operation, with those of an EMCCD, i.e. a very large number of detectors (pixels) with high quantum efficiency, low SNR and µs time resolution. We could show that our setup allows to read out fluorescence spectra from 400 to 800 nm distributed over 80 pixels with a time resolution of 12 µs and single photon counting capability. The setup benefits from the high transmission of a prism. The major drawback of a prism, the nonlinear dispersion, is accounted for in the data treatment and does not affect the data because the requirements in terms of spectral resolution are rather relaxed. Attached to a commercial CLSM, we could use our setup in solution as well as in living specimen in combination with confocal microscopy. We could confirm that spectrally resolved FCS measurements of small organic fluorophores and of quantum dots in solution agree with data acquired with conventional APD-based FCS and that they allow to recover diffusion properties and concentrations as well as to identify and distinguish more than two components with different yet overlapping spectral and diffusion properties. From a spectrally resolved analysis of fluorescence intermittence of quantum dots emitting at 655 nm we obtained additional information that can help to further elucidate the underlying processes. In addition, we could show with the first EMCDD-based spectrally resolved FCCS experiments in living cells that this approach can be used to measure molecular interactions in vivo and that it provides the required flexibility to optimize experimental conditions.

As an outlook, spectrally resolved FCS should allow to measure the formation of higher-order complexes labelled with more than two fluorophores that may even have overlapping emission spectra. Due to the spectral flexibility, overlapping detection channels can be defined to optimize the fluorescence yield whereas in combination with interleaved excitation [34, 35], cross-talk could be reduced. Also for point-scanning microscopy, such a fast spectrometer could serve as spectral detector, and the use of back-illuminated EMCCD chips with up to three-fold higher quantum efficiency should increase the sensitivity significantly. Moreover, since EMCCD-based setups have been used for spatial FCS [18–22, 36], too, our study opens the path towards combined spatially and spectrally resolved FCS, i.e. spectrally optimized imaging of interactions, transport processes and molecular dynamics in living cells.

## Acknowledgements

We would like to thank Gerrit Heuvelman, Karsten Rippe, Jérémie Capoulade and Rainer Pepperkok for helpful discussions and Katharina Müller for some help with cell culture. We are grateful to Masataka Kinjo for kindly providing the plasmids used in this study. The Dynamic Imaging Platform of IP-K and the Advanced Light Microscopy Facility of EMBL are acknowledged for their support and generous access to the microscopes as well as Leica Microsystems and Sensovation for advanced technical support.

#131620 - $15.00 USD Received 13 Jul 2010; revised 29 Sep 2010; accepted 1 Oct 2010; published 27 Oct 2010